Journal of Materials Chemistry A

Accepted Manuscript

ROYAL SOCIETY OF CHEMISTRY

www.rsc.org/materialsA

Journal Name

ARTICLE

Ultra-low content of Pt modified CdS nanorods: One-pot synthesis and high photocatalytic activity for H_2 production under visible light

Received 00th January 20xx,
Accepted 00th January 20xx

DOI: 10.1039/x0xx00000x

www.rsc.org/

Li Zhang[a], Xianliang Fu[a*], Sugang Meng[a], Xiaoliang Jiang[a], Jinghui Wang[a], Shifu Chen[a,b*]

Noble metal-modified CdS is one of the most promising photocatalyst for solar H_2 production due to its intrinsic band structure merits. It is highly desirable to develop an effective preparation route to pursue a high photocatalytic performance and to minimize the use of costly noble metals. For the first time, a simple and convenient one-pot solvothermal (OPS) method was developed to prepare platinized CdS nanorods (Pt/CdS-N) in this work. The formation of hexagonal 1D structure CdS and the deposition of Pt(0) can be achieved simultaneously by the method, which is more efficient than the conventional post-deposition routes, such as photochemical reduction and impregnation-reduction methods, to enhance the photocatalytic activity of CdS-N for H_2 evolution reaction (HER). The H_2 evolution rate (r_{H2}) of CdS-N could be remarkably improved from 2.10 to 10.29 mmol·h^{-1}·g^{-1} by loading with only 0.06% Pt (wt.%) under visible light irradiation (λ>400 nm, 300 W Xe lamp). No deactivation of the sample was observed in cyclic experiments for 20 h reaction. This loading amount of Pt is substantially lower than the reported optimal values (commonly in the range of 0.5-2%) by more than one order of magnitude. A criterion of enhancement coefficient was proposed to identify the ideal loading amount of Pt. The result indicates, considering the improvement efficiency of r_{H2} and the loading amount of Pt, this ultra-low amount of Pt is more practical than the optimal amount (determined to be 0.5%). The high and stable activity of Pt/CdS-N can be attributed to the hexagonal 1D structure of CdS and the high dispersion of Pt in the Pt(0) state. Besides Pt, the OPS method is also valid for the deposition of Pd or Ru on CdS and r_{H2} decreases in order Ru/CdS-N (12.89)>Pt/CdS-N (10.29)>Pd/CdS-N (6.72 mmol·h^{-1}·g^{-1}) with loading amount of 0.06%. It reveals that the use of noble metal co-catalyst can be significantly reduced without unduly sacrificing the HRE efficiency. The developed OPS route provides a new insight into the preparation of highly efficient and stable chalcogenide photocatalysts for HER.

1. Introduction

With the depletion of fossil fuel and the increasing concerns about its derived environmental issues, converting solar energy to a storable, renewable, and environmentally friendly H_2 fuel has been greatly stimulated in the past four decades. The most attractive route for the conversion is photocatalytic splitting water to H_2 by a semiconductor-based photocatalyst.[1] It provides a clean, sustainable, and low-cost approach for H_2 production and has been described as one of the "holy grails" of chemistry.[2] Since the first report on photo-electrochemical splitting water on TiO_2 electrode,[3] numerous efforts have been devoted to develop highly efficient photocatalyst for H_2 evolution reaction (HER),[4] especially the visible-light-responsive photocatalyst which can utilize the main part of the solar spectrum.[5] Metal chalcogenides,[6] such as CdS, In_2S_3, $ZnIn_2S_4$, and $CdIn_2S_4$, are widely regarded as potential candidates for photocatalytic HER under visible light. Among them, n-type CdS semiconductor has been intensively studied for its proper band gap (2.4 eV) and the sufficient redox potential (-0.9 V vs. NHE, pH 7) for H_2 evolution.[6a,b,7] However, synthesis CdS with controllable shape, size, crystallinity, and phase structure is still a big challenge to pursue a high and stable HER activity.

To improve the separation of photo-induced charge carriers (e^- and h^+, CCs) and increase the surface active sites for H_2 evolution, the optimizing of CdS mainly focused on its morphology, crystalline structure, and surface modification. Various morphological CdS, including nanosheets, nanorods, nanocubes, hollow spheres, microtowers, and nanotrees have been fabricated with different preparation methods.[8] One-dimensional (1D) CdS nanostructures have attracted

[a] College of Chemistry and Material Science, Huaibei Normal University, Huaibei, Anhui, China, 235000. Fax:+86 561 3090518; Tel: +86 561 3803235; E-mail: fuxiliang@gmail.com
[b] Department of Chemistry, Anhui Science and Technology University, Fengyang, Anhui, China, 233100. Fax: +86 561 3090518; Tel: +86 561 3806611; E-mail: chshifu@chnu.edu.cn

Electronic Supplementary Information (ESI) available: [XRD, UV-Vis DRS, SEM/TEM, N_2 adsorption-desorption characterizations (Fig. S1–S5); a video for reduction of $[PtCl]_6^{2-}$ in water (Video 1) and a video of H_2 evolution (Video 2).]. See DOI: 10.1039/x0xx00000x

considerable attention as the high aspect ratio structure can improve the separation of e^- and h^+ by increasing delocalization of e^- in the unique 1D structure.[9] In terms of structure, the hexagonal CdS (h-CdS) is preferred to the cubic phase. Generally, CdS in the cubic phase (c-CdS) shows a low crystallinity than that of h-CdS and contains a lot of crystal defects which can act as recombination centers for e^- and h^+.[1,4a,10] The third effective and crucial way to improve the HER activity of CdS is modifying the sample with some essential noble metal, such as Pt, Pd, or Ru.[11] These ingredients can serve as a co-catalysts to improve the trapping efficiency of photoinduced e^- and reduce the kinetic activation barrier of HER due to their large work function and the low overpotential for H_2 evolution.[12] However, the large-scale use of noble metals is strongly limited by their scarcity and the high price. Although, this problem can be partially overcame by the use of some non-noble metal co-catalysts, such as MoS_2, WS_2, NiS, $Co(OH)_2$, $Ni(OH)_2$, Cu_3P, and graphene, the HER performance and the stability of these co-catalysts are generally inferior to the noble metals and their validities are mainly confirmed by CdS.[6a,7,10,13] Whether these co-catalysts apply to other photocatalyst is still unknown. Another way to cut the cost of the co-catalyst is trying to reduce the loading amount of noble metals without a significant sacrifice in the HER activity. Considering the high efficiency and the validity of the noble metal co-catalyst have been extensively confirmed and they are widely used in photocatalytic water splitting,[12a] an attempt to devote to this study will be meaningful. This depends on a highly efficient deposition route and the exploring of the HER activity of the samples modified with low amount of noble metals.[14] Unfortunately, these attempts have been generally overlooked. Taking Pt as example, the conventional platinization of CdS is commonly achieved by photochemical reduction or impregnation-reduction methods.[11a,15] These post-deposition routes involve a series of repeated washing, centrifugation, and drying processes, and the loading amount of Pt for remarkable HER is generally in the range of 0.5-2% (wt.%, similarly hereinafter).[16] As its distribution, chemical state, and the interaction with CdS are hard to be controlled in the rapid reduction processes, Pt cannot be effectively utilized by these routes. Although, whether a significant HER activity of platinized sample can be remained at low Pt loading amount, such as in the range of 0.01-0.1%, is still inconclusive, one thing is sure that the possibility highly relies on the deposition route. Thus, to pursue a high HER activity and to cut down the amount of noble metal co-catalyst, it is highly desirable to develop a facile and effective strategy to fabricate platinized CdS. The aim of this study is to develop an efficient method to prepare high photocatalytic performance Pt/CdS through optimizing its morphology and structure, and meanwhile to minimize the use of precious Pt without substantially compromising the HER activity.

Considering the aspects of the CdS morphology, crystalline structure, and the use of noble metal co-catalyst, we developed a simple and convenient one-pot solvothermal (OPS) method for the first time in this work to prepare Pt modified CdS nanorods. The results indicated the formation of hexagonal 1D structure CdS and the deposition of Pt(0) can be achieved simultaneously by the route. More importantly, the H_2 evolution rate of pristine CdS can be remarkably enhanced from 2.10 to 10.29 $mmol \cdot h^{-1} \cdot g^{-1}$ by loading with only 0.06% Pt. Besides Pt, the OPS method is also valid for the deposition of Pd or Ru on CdS and we believe it is applicable to the preparation of other chalcogenide photocatalyst. This work reveals that the loading amount of noble metal co-catalyst can be significantly reduced without unduly sacrificing the HRE efficiency.

2. Experimental

2.1 Preparation of photocatalysts

All of the reagents were analytical grade and used as received from Sinopharm Chemical Reagent Co. High purity water was used throughout the study.

Pt/CdS-N and Pt/-CdS-P. Platinized CdS nanorods (Pt/CdS-N) were prepared by the OPS method. In a typical run, 4.66 g $Cd(NO_3)_2 \cdot 4H_2O$ and 3.45 g $CS(NH_2)_2$ (thiourea) was dissolved in 60 mL $C_2H_4(NH_2)_2$ (ethylenediamine, EDA). Then a desired amount of H_2PtCl_6 aqueous solution was added into the solution. The loading amount of Pt is controlled by varying the dosage of H_2PtCl_6 solution. If not specified, the theoretical loading amount of Pt (based on the Pt amount in the precursor) in this work is 0.06% (Pt per CdS). After stirring for about 10 min, 0.2 g $NaBH_4$ was finally added to the mixture. Quite different to in an aqueous medium, no reduction of H_2PtCl_6 is occurred in the alkaline solvent under ambient condition. The mixture solution was then transferred into a Teflon-lined stainless autoclave and kept in an oven at 160 ^oC for 48 h. The resulted yellow precipitates were collected by centrifugation and rinsed thoroughly with deionized water and absolute ethanol alternately. The final product was dried in a vacuum oven at 80 ^oC for 8 h. To confirm the high photocatalytic performance of Pt/CdS-N is partially benefited by the 1D nanostructure, platinized CdS nanoparticles (Pt/CdS-P) were also prepared by a similar OPS route with $N(C_2H_4OH)_3$ (triethanolamine, TEA) as solvent and $C_3H_7NO_2S$ (L-cysteine) as sulfur source.[9a]

In situ PR-Pt/CdS-N, PR-Pt/CdS-N, and IR-Pt/CdS-N. Besides the one-pot deposition route described here, platinized CdS-N were also prepared by some conventional post-deposition routes for comparison, including the popular *in situ* photo-reduction (*i.s.* PR), photo-reduction (PR), and impregnation-reduction (IR) deposition methods.[11b,12b,15b,17] The corresponding products were denoted as *i.s.* PR-Pt/CdS-N, PR-Pt/CdS-N, and IR-Pt/CdS-N, respectively. Specifically, pristine CdS-N was first prepared by the OPS route without dosage of H_2PtCl_6 and $NaBH_4$. As for *i.s.* PR route, the deposition procedure was similar to the HER (see section 2.3) except a required amount of H_2PtCl_6 solution was added. At the beginning of the HER reaction, Pt was deposited onto CdS-N. The resulted sample was then utilized *in situ* for the HER. For PR route, 0.5 g CdS-N was dispersed in 150 mL H_2O containing 10 mL lactic acid in the system for the HER test.

Subsequently, required amount of H_2PtCl_6 solution was added into the suspension. After deaeration, the suspension was irradiated by a 300 W Xe lamp for 3 h (PLS-SXE300, Perfect Light Co., λ>400 nm, controlled by long pass cut-off filter). The resulted precipitates were harvested by centrifugation, washing with water and ethanol several times, and finally drying in vacuum at 80 °C for 8 h. For IR method, 0.4 g prepared CdS-N was impregnated with the required amount of H_2PtCl_6 solution (ca. 2 mL) under stirring and then dried in a vacuum oven at 80 °C for 8 h. Subsequently, the resulted powders were reduced by the excess amount of 0.1 M $NaBH_4$/0.1 M NaOH mixed solution, followed by centrifugation, washing and drying processes.

(Pd, Ru)/CdS-N. To verify the applicability and validity of the OPS method, other noble metal (Pd or Ru) modified CdS-N were also prepared by the solvothermal process using $PdCl_2$ and $RuCl_3$ as the precursor, respectively, whereas other reaction conditions are unchanged.

2.2 Characterization

X-ray powder diffraction (XRD) patterns of the samples were obtained on a Bruker D8 Advance X-ray diffractometer using Ni-filtered Cu Kα radiation (λ=1.5406 Å). UV-visible diffuse reflection spectra (UV-Vis DRS) were recorded on a TU-1950 Vis-NIR spectrophotometer (TU-1950, Persee) with $BaSO_4$ as a reference. Field emission scanning electron microscopy (FE-SEM) images were observed by a Hitachi SU8000 SEM. Transmission electron microscopy (TEM) and high-resolution transmission electron microscopy (HR-TEM) images were performed on a JEM-ARM200F electron microscope operated at an acceleration voltage of 200 kV. The elemental mappings were investigated by an energy-dispersive X-ray spectrometer (EDS) attached to the TEM instrument. X-ray photoelectron spectroscopy (XPS) analysis was conducted on an ESCALAB 250 photoelectron spectrometer (Thermo Fisher Scientific) at 3.0×10^{-10} mbar using Al Kα X-ray beam (1486.6 eV). All binding energies were corrected with reference to the C 1s peak of the surface adventitious carbon at 284.6 eV. The BET surface area was determined on a Micromeritics Tristar II 3020 surface area analyzer by using N_2 adsorption data in the relative pressure (P/P_0) range of 0.05–0.25. The deposition amounts of Pt, Pd and Ru on CdS-N were analysed by inductively coupled plasma absorption electron spectroscopy (ICP-AES) on a Varian 720-ES unit. The powder samples were digested by a mixture of HNO_3 and HCl under microwave irradiation. The ICP signal intensities were calibrated by a multi-elemental ICP standard solution (containing of Au, Pd, Pt, Ir, Ru, Aladdin Reagent Co., China). Photoluminescence (PL) emission spectra of platinized CdS-N were recorded on a JASCO FP-6500 type fluorescence spectrophotometer excited by 420 nm light at room temperature. The photocurrents of the prepared samples were recorded on a CHI 660E electrochemical workstation (Chenhua, Shanghai) at a bias of 0.1 V (vs. SCE) in a standard three-electrode cell with the samples as the working electrode, a Ag/AgCl electrode (in 3M KCl solution) as the reference electrode, and a Pt gauze as the counter electrode, respectively. The thin film working electrodes (0.6×0.6 cm^2) were prepared by drop-casting samples/ethanol suspensions onto FTO glass substrates followed by drying the film at 60 °C overnight. 0.1 M Na_2SO_4 aqueous solution was used as the electrolyte. The aforementioned 300 W Xe lamp (λ>400 nm) was used as the light source.

2.3 Photocatalytic HER test

Photocatalytic HER experiments of the prepared samples were conducted on a commercial reaction system (LabSolar II, Perfect Light Co.). A Pyrex top-irradiation reaction cell was used as a reactor. In a typical experiment, 50 mg sample was suspended in a mixture of 90 mL water and 10 mL lactic acid (used as sacrificial reagent). The system was then degassed by a mechanical pump. Before irradiation, the suspension was stirred in the dark for 30 min to establish an adsorption-desorption equilibrium. Aforementioned 300 W Xe lamp (λ>400 nm) was used as the light source. The solution temperature was controlled at ca. 5 °C by a water cooling system. The generated H_2 was measured by an online gas chromatograph (GC7900, TianMei, Shanghai) equipped with a TCD detector and a molecular sieve 5A column using Ar as carrier gas.

3. Results and discussion

3.1 X-ray diffraction study

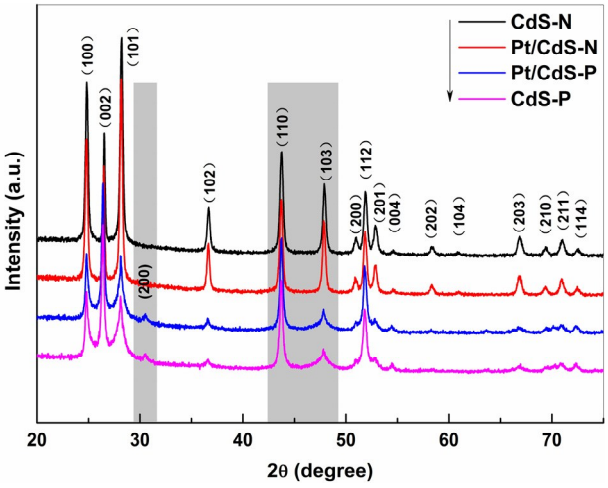

Fig. 1 XRD patterns of CdS-N, CdS-P, and the corresponding platinized samples prepared by the OPS method.

Fig. 1 shows the XRD patterns of the pristine CdS-N, CdS-P, and the corresponding platinized samples prepared by the OPS method. All the diffraction peaks of CdS-N and Pt/CdS-N can be well indexed to the standard h-CdS (hexagonal CdS) with lattice parameters of a=4.1 and c=6.7 Å (JCPDS No. 41-1049). The samples are in a highly crystalline wurtzite structure and no peak originating from impurities or c-CdS (cubic phase) is detected. However, CdS-P and Pt/CdS-P show a mixed phase of h- and c-CdS. Besides the diffraction peaks of h-CdS, a small peak corresponding to the (200) plane of c-CdS (JCPDS No. 80-0019) can be found at 2θ=30.7°. As the theoretical loading amount of Pt is only 0.06%, the platinized CdS-N and CdS-P

show identical diffraction pattern to the pristine CdS samples and no Pt-derived peaks can be perceived, which commonly locate at 40.0 and 46.5°.[18] These phenomena can also be observed in (Pd, Ru)/CdS-N samples (Fig. S1, see the electronic supplementary information, ESI). As shown in Fig. 1, the diffraction peaks of CdS-N and Pt/CdS-N are more intensive than that of CdS-P and Pt/CdS-P, suggesting CdS nanorods get higher crystallinity than CdS particles. It can be further confirmed by calculating the peak intensity ratio of (103) and (110) planes. This value has been used to infer the composition and estimate the crystallinity of wurtzite CdS.[19] The calculation indicates the ratios are 0.67 and 0.21 for CdS-N and CdS-P, respectively, indicating the nanorods CdS samples are well crystalized.

3.2 UV-vis diffuse reflection spectra

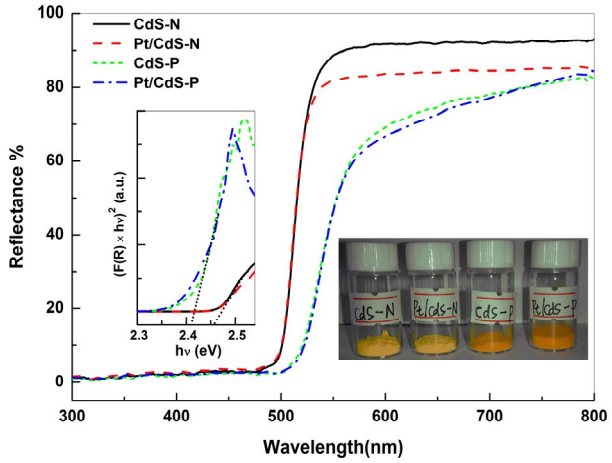

Fig. 2 UV-vis DRS of CdS-N, CdS-P, and the corresponding platinized samples. The inset is their corresponding photos (right) and the Tauc plots (left) of the transformed Kubelka–Munk function $(F(R)\times h\nu)^2$ vs. hν.

Fig. 2 shows the UV-vis DRS spectra of prepared CdS and the platinized samples. A strong absorption edge at ca. 500 nm can be found in the hexagonal structure of CdS-N due to the intrinsic band gap transition, while for CdS-P in the mixture of cubic and hexagonal phase, it shows a strong absorption onset at ca. 515 nm. In comparison to CdS-P, CdS-N shows a slight blue shift of the absorption. The different absorption feature of CdS-N and CdS-P is consistent with their color change, from light yellow to orange as shown in the bottom inset of Fig. 2. Apparently, the band gap transitions of CdS are not affected by the platinization as the absorption edges are unchanged. It suggests the deposition of Pt is a modification process rather than a lattice doping. However, as shown in Pt/CdS-N and Pt/CdS-P, the absorption in the visible light range (600-800 nm) is slightly improved due to the presence of Pt.[15b,17,20] Similar results can also be achieved for Pd or Ru modified CdS-N (Fig. S2). Tauc's formula[21] was used to determine the band gap energy (E_g) of the prepared CdS samples: $K(h\nu-E_g)^{1/n} = F(R)h\nu$, where F(R) is the absorption coefficient (calculated by the Kubelka-Munk function), hν is photon energy, K is a constant, and n equals 2 for direct transition and 1/2 for indirect transition. Since CdS is a direct band gap material, n=2 was used to generate the Tauc plots. As shown in the left inset of Fig. 2, .the band gap of CdS-N and CdS-P are 2.46 and 2.41 eV, respectively, and are comparable to the band gap energy of bulk CdS (2.42 eV).[19b] The different absorption feature between CdS-N and CdS-P can be attributed to their different morphology (see section 3.3) and the phase structure (Fig. 1).[15d,22] Some previous studies also indicated the E_g of a hexagonal structure CdS is larger than that of a cubic one.[8f]

3.3 Morphology

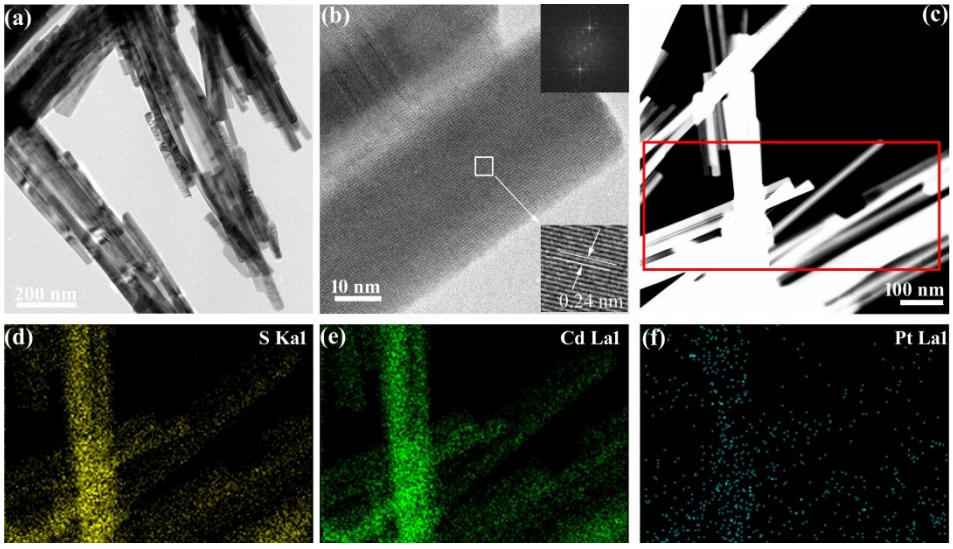

Fig. 3 (a) TEM image, (b) HRTEM, (c) HAADF-STEM image, and (d-f) EDS mapping of the prepared Pt/CdS-N. The top right inset of (b) shows the FFT image of the nanorods.

The morphology of the prepared Pt/CdS-N was characterized by TEM and SEM (Fig. 3 and S3). Well-aligned CdS nanorods can be observed with a length of 1-5 μm (Fig. S3) and a diameter of ca. 35 nm (Fig. 3a and b). A set of crystal lattice fringes with a d spacing of 0.24 nm is disclosed in the HRTEM image (Fig. 3b), which can be ascribed to the (102) planes of h-CdS. The fast Fourier transforms (FFT) image (in the top right inset of Fig.3b) demonstrates the nanorods are in single crystalline nature. The surface of the nanorods is quite smooth and the decoration of Pt particles on the CdS nanorods cannot be observed even in the more distinguishable high-angle annular dark field scanning image (HAADF-STEM, Fig. 3c).[20,23] It implies Pt may be highly dispersed on the nanorods in a cluster form with a subnanometer size,[23,24] although the size is still unknown at present. The smooth surface feature of Pt/CdS-N is further confirmed by the SEM images (Fig. S3-b). To study the dispersion of S, Cd and Pt, EDS elemental mapping analysis of the rectangle area shown in Fig. 3c was conducted (Fig. 3d-f). All the mapping images present the same profile as that shown in the rectangle area (Fig. 3c). It indicates the constituting elements including Pt, S, and Cd are homogeneous distributed on the nanorods. As shown in Fig. 3f, the spots originated from the Pt particles are fairly small and are spread randomly throughout the nanorods, further suggesting Pt is finely dispersed. The SEM image (Fig. S3-c) of Pt/CdS-P indicates the sample is composed by nanoparticles with no distinctive morphology. The average size of the particles is ca. 100 nm. As shown in Fig. S4, the morphology of CdS-N sample is not affected by the deposition of Pd, Pt, or Ru and maintains a rod-like structure.

3.4 XPS analyses

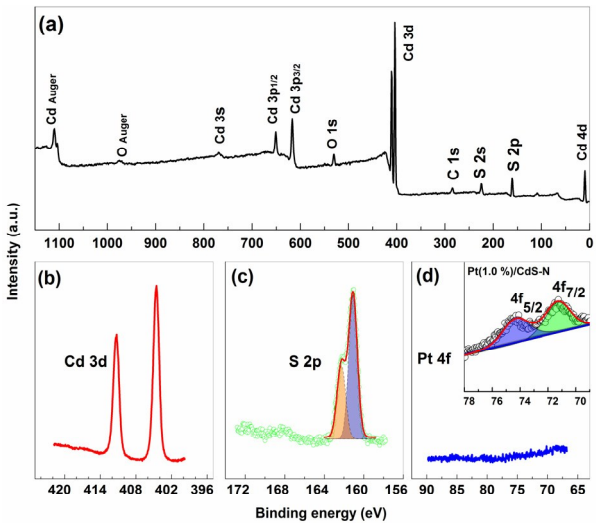

Fig. 4 (a) survey and high resolution (b) Cd 3d, (c) S 2p, and (d) Pt 4f XPS spectra of prepared Pt/CdS-N. The inset of (d) shows the Pt 4f spectrum of the sampled loaded with 1.0 % Pt.

XPS was used to study the surface composition and the chemical states of the elements in Pt/CdS-N. As shown in Fig. 4a, besides the adventitious C and the adsorbed O, the sample is composed of Cd and S. No Pt signal can be perceived in the survey spectrum due to the ultra-low deposition amount of Pt. The characteristic N 1s signal (at ca. 397 eV) cannot be observed suggesting EDA has been removed completely by the washing process. The atomic ratio of Cd to S is 1.04, close to the nominal composition of CdS. Two peaks centered at the binding energy (BE) of 404.5 (Cd $3d_{5/2}$) and 411.2 (Cd $3d_{3/2}$) eV can be found in the high resolution spectrum of Cd 3d (Fig. 4b). The BE values and the splitting energy of 6.7 eV are consistent with the reported results of Cd^{2+} in CdS.[25] The spectrum of S 2p (Fig. 4c) indicates the peak can be deconvoluted into two peaks, one located at ca. 161.0 and the other at ca. 162.1 eV. The signals can be attributed to S^{2-} in CdS.[49,25b] Due to the detection limit of XPS, the Pt 4f peaks still cannot be found even in the high resolution spectrum (4d). Generally, the spectrum is composed of Pt $4f_{7/2}$ and Pt $4f_{5/2}$ with a separation of 3.3 eV due to the spin orbit coupling.[26] The BE value of Pt $4f_{7/2}$ is around 71.1, 72.4 and 74.2 eV for Pt(0), Pt^{2+} and Pt^{4+}, respectively,[27] and changes with the chemical state of Pt. To explore the chemical states of the deposited Pt, 1.0% Pt modified CdS-N was deliberately prepared by the OPS method through increasing the dosage of H_2PtCl_6 solution. The high resolution Pt 4f spectrum was then measured. As shown in the inset of Fig. 4d, a doublet peak centered at 71.2 (Pt $4f_{7/2}$) and 74.4 eV (Pt $4f_{5/2}$) can be found. Apparently, the BE values are close to that of Pt(0), suggesting the Pt precursor can be successfully reduced to the metallic state by the one-pot route. Thus, it is reasonable to infer that the deposited Pt in Pt/CdS-N (with only 0.06% Pt deposition amount) is also in the Pt(0) state. This state of Pt is an important prerequisite for highly efficient HER as it provides more active sites than the Pt^{2+} and Pt^{4+}.[17,20]

3.5 Photocatalytic activity

The HER activity of the prepared samples was compared under visible light irradiation (>400 nm) using lactic acid as the electron donor. Control tests indicate no H_2 was produced in the absence of photocatalyst or irradiation, suggesting the evolution of H_2 is triggered by a photocatalytic process. As shown in Fig. 5, a linear increase of H_2 with irradiation time can be found for all tests. Thus, the HER rates (r_{H2}) of the samples can be calculated according to the fitting lines' slopes and the results are compared in Fig. 6.

Apparently, nanorods CdS samples (Fig. 6b-d) show much higher activity than that of nanoparticles CdS samples (Fig. 6a). Although the surface area of CdS-P (36.5 $m^2 \cdot g^{-1}$, summarized in Table. 1) is substantially larger than that of CdS-N (26.1 $m^2 \cdot g^{-1}$, determined by the N_2 adsorption data shown in Fig. S5), the r_{H2} of pristine CdS-P is only 0.28 $mmol \cdot h^{-1} \cdot g^{-1}$ (Fig. 6a) and it is significantly lower than that of pristine CdS-N (2.10 $mmol \cdot h^{-1} \cdot g^{-1}$, Fig. 6b). After deposition of only 0.06% Pt by the OPS method, the activities of CdS-P and CdS-N were substantially improved, from 0.28 to 1.02 and 2.10 to 10.29 $mmol \cdot h^{-1} \cdot g^{-1}$, respectively. It clearly suggests the BET surface area cannot fully account for the different activity between CdS-N and CdS-P. A control test indicates, if $NaBH_4$ was not used in the preparing of Pt/CdS-N, the r_{H2} of resulted sample is only 1.96 $mmol \cdot h^{-1} \cdot g^{-1}$, a value almost identical to the r_{H2} of bare CdS-N. It implies no Pt species were loaded on CdS-N. Otherwise, the

activity will be improved to some extent. Thus, the reductant of $NaBH_4$ is indispensable for the deposition of Pt in the OPS route.

Several factors are responsible for the high HER performance of CdS-N. First, it is the unique 1D structure of the nanorods. The transferring and separation of photoinduced CCs can be facilitated by this 1D structure.[9a, 28] Second, it is the highly crystalized structure. As the recombination of photo-induced CCs can be significantly promoted by structural defects, the crystallinity becomes a critical factor for high photocatalytic activity, especially for HER.[1,4a,10] The last factor is the crystalline phase. Reported works[8f,10,29] indicated the h-CdS showed higher photocatalytic activity than the c-CdS or the mixture of hexagonal and cubic CdS. Since CdS-N is in high crystalized hexagonal phase with 1D structure and CdS-P is in a mixture phase of hexagonal and cubic, no wonder high HER activity is observed over CdS-N samples.

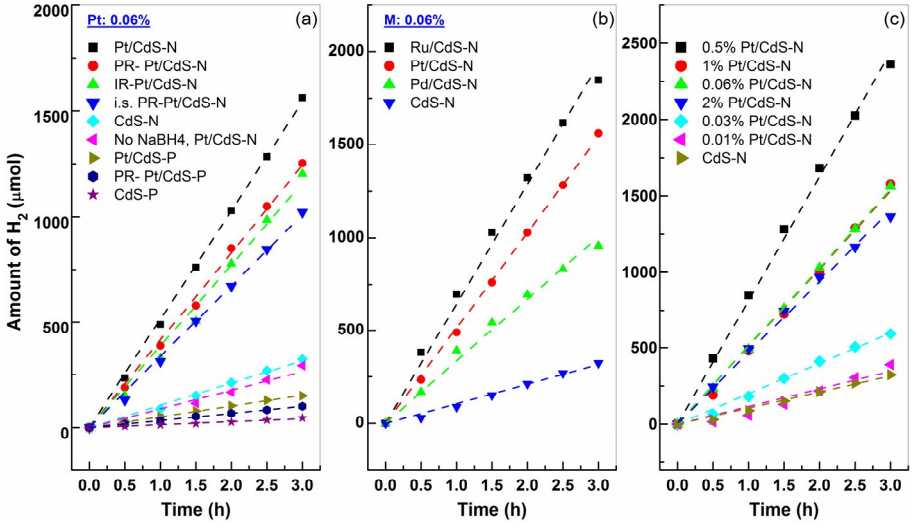

Fig. 5 The time courses of H_2 evolution under visible irradiation (>400 nm) over (a) CdS-N, CdS-P and their platinized samples, (b) different noble metal-modified CdS-N, and (c) different amount of Pt modified CdS-N.

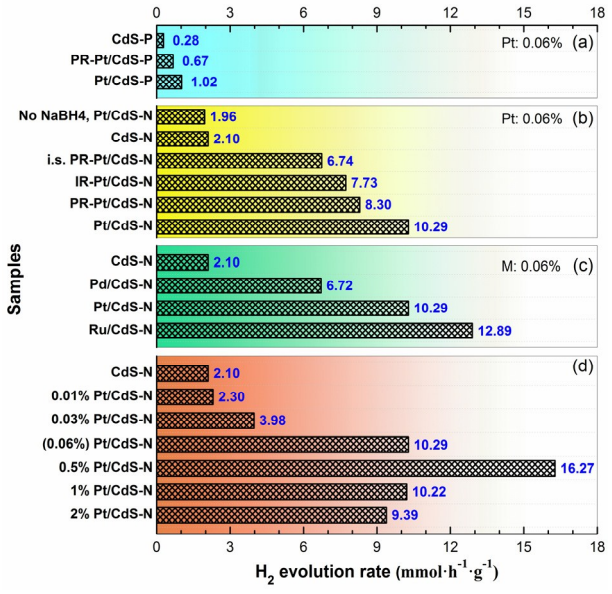

Fig. 6 Comparison of H_2 evolution rates of: (a) CdS-P and platinized CdS-P samples, (b) CdS-N and platinized CdS-N (0.06% Pt) samples prepared by different deposition routes, (c) different noble metal-modified CdS-N (0.06% M, M=Pt, Pd, or Ru) and (d) different amount of Pt modified CdS-N samples prepared by the OPS method.

As shown in Fig. 6b, the r_{H2} of the platinized CdS-N prepared by *i.s.* PR, IR and PR routes are only 6.74, 7.73, and 8.30 $mmol \cdot h^{-1} \cdot g^{-1}$, respectively. Obviously, the simple and convenient OPS method is more effective than the post-deposition routes to improve the HER activity of CdS-N. The phenomenon can be observed on CdS-P as well to a certain extent. The r_{H2} of PR-Pt/CdS-P is only 0.67 $mmol \cdot h^{-1} \cdot g^{-1}$, lower than that of Pt/CdS-P (1.02 $mmol \cdot h^{-1} \cdot g^{-1}$) prepared by the similar OPS procedure.

The primary advantage of the OPS method is that Pt is deposited by a gentle process in a "mild" solvent (EDA or TEA). As we known, $NaBH_4$ is quite unstable in an aqueous solution[30] and the reduction of $[PtCl_6]^{2-}$ can be quickly achieved by its breakdown products, i.e. atomic hydrogen. As the decomposition of $NaBH_4$ can be further catalyzed by the resulted Pt particles, the reduction process will be self-accelerated and finished in a short time, leading to a failure to control the deposition of Pt. As shown in the video clip (Video 1, see the ESI), a control test indicates the deposition of Pt in aqueous solution can be promptly achieved in 30 s. However, when the reduction is performed in EDA or TEA, the hydrolysis of $NaBH_4$ can be suppressed in the alkaline and water deficient solvents.[30] Indeed, no decomposition of $NaBH_4$ has been observed at room temperature in the OPS processes. Furthermore, as the amines can serve as ligands, a complex can be formed between $[PtCl_6]^{2-}$ and the amines,[31] retarding the reduction of Pt precursor. These factors determine, along with the formation of CdS, the reduction of Pt will be achieved gently with the decomposition of $NaBH_4$ caused by elevating the solvothermal temperature, which provides a uniform

deposition of Pt. Furthermore, the elevated temperature can strengthen the contact between Pt and CdS-N, and consequently benefits the immigration of e^- from CdS-N to Pt. These are the reasons why the OPS route is more effective than the conventional deposition routes to improve the HER activity of CdS-N.

The assumption about the deposition process of Pt on CdS-N is tentatively confirmed by the observation of the reaction. To visualize the formation of CdS and the deposition of Pt, a parallel preparation reaction was performed in a two-necked flask heated by oil bath. A high dosage of H_2PtCl_6 solution (corresponding to 1% loading amount) was used intentionally to highlight the change of the reaction. A picture was taken for every 10 °C increase in the oil temperature. As shown in Fig. 7, unlike in aqueous medium, no reaction was observed at the temperature below 50 °C, never mind at room temperature. Some light yellow particles were formed on the flask wall when the temperature reaches 60 °C (indicated by the arrow) and the amount increased with further increases temperature to 90 °C, suggesting the nucleation of CdS. When the temperature reaches 100 °C, some small bubbles (indicated by the arrow) appear and the solution color changes to light brown, suggesting the decomposition of $NaBH_4$ and the reduction of $[PtCl_6]^{2-}$. As the temperature further increased to 130 °C, more and more bubbles appear and the clear solution becomes cloudy and gradually changes to dark brown due to the accumulation of CdS and the deposition of Pt. The depletion of $NaBH_4$ is accomplished at 140 °C indicated by the disappearing of the foams. Instead, some big bubbles come out at this temperature and become more intense at 150 °C due to the boiling of the EDA (its boiling point is ca. 120 °C). The delay of the heat transfer accounts to the boiling lag. This result convincingly demonstrates the formation of CdS and the deposition of Pt are processed almost simultaneously and compared to in H_2O, the reduction of $[PtCl_6]^{2-}$ by $NaBH_4$ can be substantially retarded by in EDA.

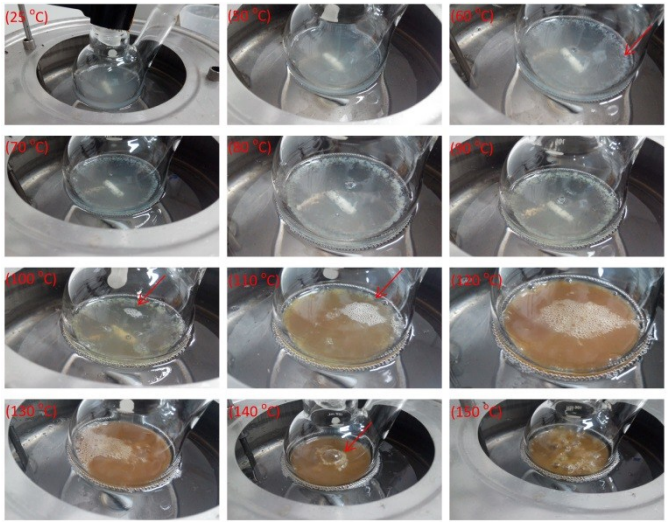

Fig. 7 Images illustrating the formation process of 1% Pt/CdS-N prepared by the OPS route. The reaction was performed in a two-necked flask heated by oil bath. The pictures were taken for every 10 °C increase in the oil temperature

To further evaluate the applicability of the OPS route, Pd and Ru, the other two commonly used co-catalysts were deposited on CdS-N, respectively, by the method at the nominal loading amount of 0.06%. As shown in Fig. 6c, the HER activity of CdS-N can be enhanced about 3-6 times by the modifications. The r_{H2} of the M/CdS-N (M=Pt, Pd, or Ru) samples decreases in order Ru/CdS-N (12.89)>Pt/CdS-N (10.29)>Pd/CdS-N (6.72 $mmol \cdot h^{-1} \cdot g^{-1}$). Ru/CdS-N shows even higher activity than Pt modified CdS-N. It may be explained by the finding that the practical loading amount of Ru (0.056%) is larger than that of Pt (0.014%) and Pd (0.037%), and is close to the theoretical value of 0.06%. The high deviation of Pt amount is caused by the fact that the ICP emission signal of Pt is disturbed by Cd signal.[32] For Ru and Pd, no such problem exists. In addition, due to the formation of the complex between $[PtCl_6]^{2-}$ and the EDA,[31] the loss of some Pt precursor may be occurred. Thus, according to the improved HER activities, the validity and reproducibility of the OPS method for the deposition of noble metals can be largely approved by this result. For easy reference, the morphologies, BET surface areas, r_{H2}, and the loading amount of noble metal of the CdS and modified CdS samples prepared by the OPS route were summarized in Table 1. A video recording (Video 2) of HER over Pt/CdS-N is given in the ESI.

Table 1 Summarize the characterization results of CdS samples prepared by the OPS route.

Samples[a]	Morphology	S_{BET} ($m^2 \cdot g^{-1}$)	r_{H2} ($mmol \cdot h^{-1} \cdot g^{-1}$)	M% (ICP)
CdS-P	NPs[b]	36.5	0.28	-
Pt/CdS-P	NPs	27.1	1.02	-
CdS-N	NRs[c]	26.1	2.10	-
Pt/CdS-N	NRs	24.0	10.29	0.014
Pd/CdS-N	NRs	24.9	6.72	0.037
Ru/CdS-N	NRs	24.1	12.89	0.056

[a] the nominal loading amount of the noble metal is 0.06%. [b] Nanoparticles. [c] Nanorods

To determine the ideal loading amount of Pt, a series of platinized CdS-N was prepared by the OPS method. The influence of the Pt amount on the r_{H2} is shown in Fig. 6d. It shows that the r_{H2} of CdS-N can be significantly improved by the deposition of a little amount of Pt (from 0 to 0.5%). The sample loaded with 0.5% Pt shows the highest HER activity and the r_{H2} is as high as 16.27 $mmol \cdot h^{-1} \cdot g^{-1}$. This value is almost 8 times higher than that of pristine CdS-N (2.1 $mmol \cdot h^{-1} \cdot g^{-1}$). A decay of the r_{H2} can be found by further increasing the Pt loading amount from 0.5 to 2%. It may be caused by the light shielding effect of Pt.[16a,20] Due to the covering of the photoactive sites by the excessive Pt, a low generation of CCs will be resulted. As shown in Fig. S6, the visible absorbance of the platinized CdS-N increases with Pt amount, suggesting the existence of the shielding effect. Furthermore, the excessive Pt may serve as a charge recombination center[33] and jeopardizes

the HER. Due to these side effects, the Pt amount is not the more the better. The practical loading amount of Pt must be optimized to pursue high HER activity.

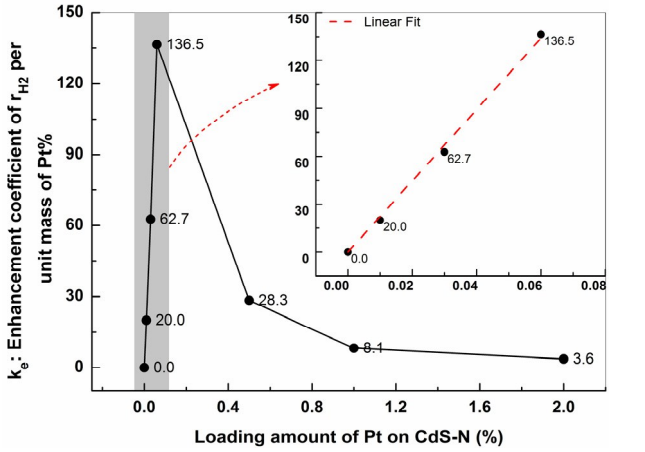

Fig. 8 Plot of the enhancement coefficient of r_{H2} per unit mass of Pt% (k_e) vs. the loading amount of Pt (%) on CdS-N.

Apparently, if simply judging from r_{H2}, the optimal loading amount of Pt in here is 0.5%. However, considering the high price of Pt and its scarcity, this loading amount may be impractical. The ideal loading amount of Pt is determined by the balance between the enhancement efficiency of the r_{H2} and the Pt loading amount. To reveal this ideal loading value and evaluate the utilization of Pt, a criterion of the enhancement coefficient of r_{H2} per unit mass of Pt% (k_e) was proposed, which is calculated by Eq. 1 based on the data shown in Fig. 6d:

$$r_{H2} = 2.1 + k_e \times M_{Pt\%} \quad \text{(Eq. 1)}$$

where $M_{Pt\%}$ is the nominal loading amount of Pt (in percentage terms), r_{H2} is the H_2 evolution rate of the corresponding platinized CdS-N, 2.1 is the r_{H2} value of pristine CdS-N. The enhancement efficiency of Pt can be evaluated by k_e. As shown in Fig. 8, the k_e value increases linearly and steeply with Pt amount from 0 to 0.06% (magnified in the inset of Fig. 8) and reaches a maximum value of 136.5 on the sample Pt/CdS-N (0.06% Pt). The linear relationship suggests Pt is highly dispersed and the enhancement of r_{H2} directly depends on the loading amount of Pt, i.e. the number of the active sites for H_2 evolution. The linear fitting result indicates the linear correlation coefficient between k_e and Pt% is 2232.6. However, when Pt amount exceeds 0.06%, an exponential decay of k_e can be observed and the value then gradually approaches to a constant at Pt loading amount of 1-2%. The decay of k_e suggests, in high loading amount range, Pt cannot be efficiently utilized as a co-catalyst for HER due to its side effects and the aggregation of Pt. Although the sample loaded with 0.5% Pt shows the highest HER activity, the k_e on the sample is only 28.3 and it is about one-fifth of Pt/CdS-N. It suggests Pt was not fully utilized in this sample. Thus, from this perspective, the Pt loading amount of 0.06% is more practical than that of 0.5%. This ultra-low loading amount of Pt cannot only reduce the cost of the photocatalyst, but also can significantly improve the HER activity. A comparison of the HER efficiency of the platinized CdS-N samples with the reported CdS based photocatalysts is present in Table. S1 (see the ESI). Apparently, the HER activity of the samples prepared in this work by the developed OPS route is quite impressive among the reported samples, especially Pt/CdS-N loaded with only of 0.06% Pt.

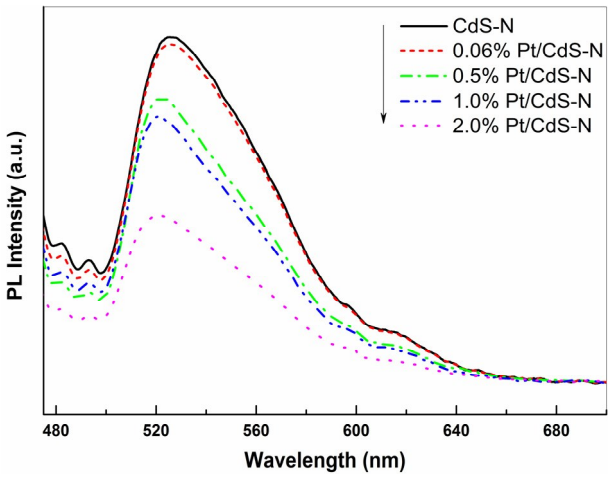

Fig. 9 PL emission spectra of pristine CdS-N and the platinized CdS-N with different loading amount of Pt.

The separation efficiencies of photo-induced e^- and h^+ on the platinized CdS-N samples were investigated by PL analysis. The PL emission mainly arises from the recombination of the CCs and the intensity is proportional to the generation rate of CCs and their subsequent recombination rate. These two factors determine the final PL intensity. As shown in Fig. 9, a band edge emission around 520 nm can be observed for all samples. The PL intensity obtained over the platinized samples is weaker than that of pristine CdS and decrease with the loading amount of Pt. For the sampled loaded with only 0.06% Pt, the decay of the emission peak is mainly caused by the retardation of the recombination of CCs. However, for high Pt-loaded samples (0.5-2.0%), the decay cannot be induced only by the retardation. If the low PL emission were simply contributed by the suppression of the recombination of CCs, an improvement of r_{H2} would be observed. Apparently, the conclusion contradicts to the data shown in Fig. 5c and Fig. 6d because a reduction of r_{H2} was observed with increasing of Pt amount. That suggests the generation of CCs is hampered on these samples due to the shielding effect of excessive Pt, which is also responsible for the decay of the PL emission. Thus, the existence of the shielding effect of Pt on the high Pt-loaded sample can be further confirmed by this result.

The photo-corrosion of chalcogenides in HER is a well-known issue. Besides its high activity, the stability of prepared Pt/CdS-N was further confirmed by cyclic experiments. Four successive runs were conducted without renewing the solution and the photocatalyst. After each run, the evolved H_2 was removed by evacuation. In general, as shown in Fig. 10, a linear increase of H_2 with irradiation time can be observed in each run. The linear fitting lines are almost parallel to each other. In the 3rd and 4th run, a slight drop of r_{H2} can be found,

which may be caused by the consumption of lactic acid. To confirm this possibility, the solution after the 4th run was supplemented by 5 mL lactic acid and a recovery of r_{H2} can be observed in the 5th run, justifying the assumption. Besides, with the proceeding of the HER, we noted some Pt/CdS-N particles were adhered to the reactor wall (above the solution level) caused by the stirring and the bubbling of H_2 (see the Video 2 in the ESI). Thus, this part of the sample did not involve in the HER in the subsequent runs, which may also account for the slight drop of r_{H2}. Similar phenomenon has been observed in photocatalytic oxidation process.[34] Thus, the stability of Pt/CdS-N can be largely approved by the cyclic experiments. The robustness of the sample is further confirmed by the XRD, Uv-vis DRS, and SEM results of the used sample (measured after the 5 runs test). As shown in Fig. 11, the XRD and DRS patterns of the used sample are identical to the fresh one and the used sample still has a rod-like structure, with nearly the same length and diameter as the fresh one. Thereby, the structural and the morphologic stability of the prepared Pt/CdS-N can be confirmed by this result.

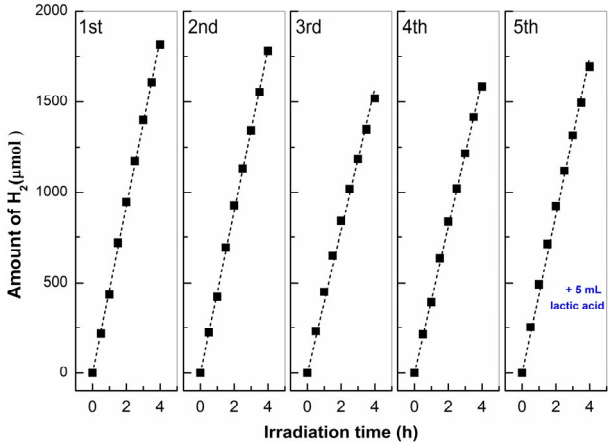

Fig. 10 Successive test runs for HER on Pt/CdS-N under visible light irradiation.

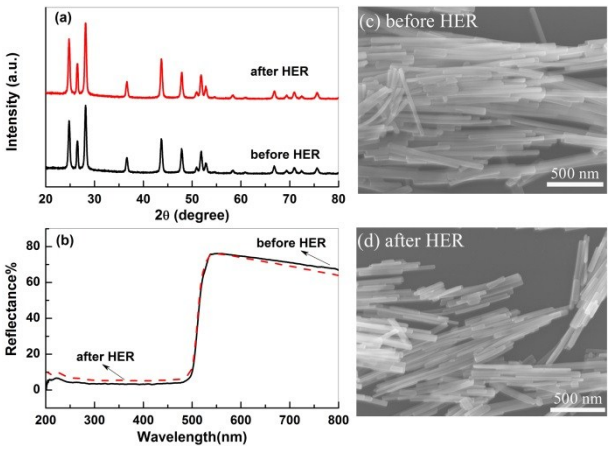

Fig. 11 (a) XRD, (b) UV-vis DRS spectra, and (c, d) SEM images of the Pt/CdS-N samples before and after HER test.

3.6 Photo-electrochemical analyses

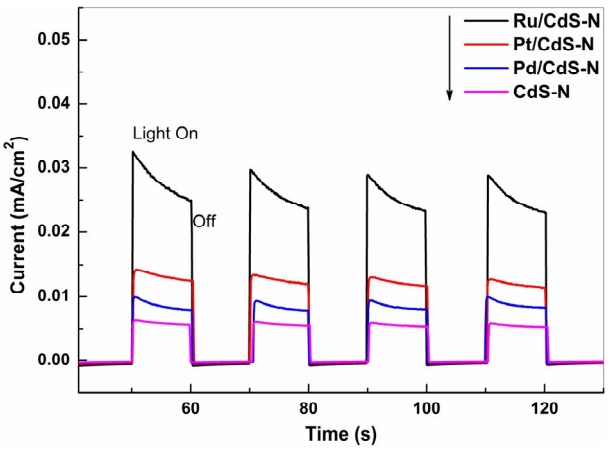

Fig. 12 Comparison the photocurrent responses of M/CdS-N samples (M=Pt, Pd, or Ru) under visible irradiation

Photo-electrochemical methods can be used to qualitatively study the excitation and transferring of photo-generated CCs. To understand the HER performances of the prepared M/CdS-N, the transient photocurrent responses of these samples were recorded under visible light illumination for several on-off cycles. As shown in Fig. 12, a quick response of the photocurrent can be found on the samples and the current values are reproducible during several intermittent on-off irradiation cycles. The stable photocurrents decrease in order Ru/CdS-N>Pt/CdS-N>Pd/CdS-N>CdS-N. The sequence is consistent with their HER performance. Obviously, the modified CdS-N samples show higher photocurrent than the pristine CdS-N. It suggests the deposition of noble metal is conducive to the transferring and separation of photo-induced CCs, even their theoretical loading amount is only 0.06%. This enhancement can highly improve the photocatalytic performance for HER.

Conclusions

In summary, we have successfully developed a simple and convenient one-pot solvothermal method to prepare Pt modified CdS nanorods. The formation of CdS nanorods and the deposition of Pt(0) could be achieved simultaneously by the route. Photocatalytic HER results indicate the deposition route is more effective to enhance the HER activity of CdS-N than the commonly used post-deposition routes, such as the popular in situ photo-reduction, photo-reduction, and impregnation-reduction deposition routes. Although the sample loaded with 0.5% Pt shows the highest HER activity (16.27 $mmol \cdot h^{-1} \cdot g^{-1}$), from the perspective of the enhancement coefficient, the ideal loading amount of Pt should be only 0.06% (10.29 $mmol \cdot h^{-1} \cdot g^{-1}$) as Pt can be fully dispersed and utilized and its side effects can be minimized. The unique 1D nanorods structure of hexagonal CdS and the promotion effect of Pt accounts for the high and stable activity. Besides Pt, the OPS method is also valid for the deposition of Pd or Ru. It reveals that, via the OPS route, the loading amount of noble metal co-catalyst can be significantly reduced without unduly sacrificing

the HRE efficiency. We also anticipate that this simple and convenient one-pot solvothermal method is also applicable to the preparation of other noble metal-modified chalcogenide photocatalyst.

Acknowledgements

This work was financially supported by the Natural Science Foundation of China (Grant Nos. 21473066, 51272081, and 51472005), the Natural Science Foundation of Anhui Province, China (Grant Nos. 1408085QB38), and the High Education Revitalization Plan of Anhui province, China.

Notes and references

1 X. Chen, S. Shen, L. Guo, S. S. Mao. *Chem. Rev.,* 2010, **110**, 6503.
2 A. J. Bard, M. A. Fox. *Acc. Chem. Res.,* 1995, **28**, 141.
3 A. Fujishima, K. Honda. *Nature,* 1972, **238**, 37.
4 (a) A. Kudo, Y. Miseki. *Chem. Soc. Rev.,* 2009, **38**, 253. (b) F. E. Osterloh. *Chem. Mater.,* 2008, **20**, 35.
5 (a) X. Wang, K. Maeda, A. Thomas, K. Takanabe, G. Xin, J. M. Carlsson, K. Domen, M. Antonietti. *Nat. Mater.,* 2009, **8**, 76. (b) R. Asahi, T. Morikawa, T. Ohwaki, K. Aoki, Y. Taga. *Science,* 2001, **293**, 269. (c) Z. G. Zou, J. H. Ye, K. Sayama, H. Arakawa. *Nature,* 2001, **414**, 625. (d) K. Maeda, K. Teramura, D. Lu, T. Takata, N. Saito, Y. Inoue, K. Domen. *Nature,* 2006, **440**, 295.
6 (a) X. Zong, H. J. Yan, G. P. Wu, G. J. Ma, F. Y. Wen, L. Wang, C. Li. *J. Am. Chem. Soc.,* 2008, **130**, 7176. (b) Q. Li, B. Guo, J. Yu, J. Ran, B. Zhang, H. Yan, J. R. Gong. *J. Am. Chem. Soc.,* 2011, **133**, 10878. (c) X. Fu, X. Wang, Z. Chen, Z. Zhang, Z. Li, D. Y. C. Leung, L. Wu, X. Fu. *Appl. Catal. B Environ.,* 2010, **95**, 393. (d) B. Xu, P. He, H. Liu, P. Wang, G. Zhou, X. Wang. *Angew. Chem.,* 2014, **53**, 2339. (e) B. B. Kale, J. O. Baeg, S. M. Lee, H. Chang, S. J. Moon, C. W. Lee. *Adv. Funct. Mater.,* 2006, **16**, 1349.
7 T. Simon, N. Bouchonville, M. J. Berr, A. Vaneski, A. Adrovic, D. Volbers, R. Wyrwich, M. Doblinger, A. S. Susha, A. L. Rogach, F. Jackel, J. K. Stolarczyk, J. Feldmann. *Nat. Mater.,* 2014, **13**, 1013.
8 (a) Y. Xu, W. W. Zhao, R. Xu, Y. M. Shi, B. Zhang. *Chem. Commun.,* 2013, **49**, 9803. (b) G. Menagen, J. E. Macdonald, Y. Shemesh, I. Popov, U. Banin. *J. Am. Chem. Soc.,* 2009, **131**, 17406. (c) W. Yang, Y. Liu, Y. Hu, M. Zhou, H. Qian. *J. Mater. Chem.,* 2012, **22**, 13895. (d) M. Luo, Y. Liu, J. Hu, H. Liu, J. Li. *ACS appl. Mat. Interfaces,* 2012, **4**, 1813. (e) Y. P. Xie, Z. B. Yu, G. Liu, X. L. Ma, H. M. Cheng. *Energy Environ. Sci.,* 2014, **7**, 1895. (f) J. Yu, Y. Yu, B. Cheng. *RSC Adv.,* 2012, **2**, 11829. (g) D. Wang, D. Li, L. Guo, F. Fu, Z. Zhang, Q. Wei. *J. Phys. Chem. C,* 2009, **113**, 5984. (h) M. Muruganandham, Y. Kusumoto, C. Okamoto, A. Muruganandham, M. Abdulla-Al-Mamun, B. Ahmmad. *J. Phys. Chem. C,* 2009, **113**, 19506.
9 (a) J. Yu, Y. Yu, P. Zhou, W. Xiao, B. Cheng. *Appl. Catal. B Environ.,* 2014, **156-157**, 184. (b) B. Weng, S. Q. Liu, N. Zhang, Z. R. Tang, Y. J. Xu. *J. Catal.,* 2014, **309**, 146. (c) T. Zhai, X. Fang, L. Li, Y. Bando, D. Golberg. *Nanoscale,* 2010, **2**, 168.
10 Q. Li, X. Li, S. Wageh, A. A. Al-Ghamdi, J. Yu. *Adv. Energy Mater.,* 2015, **5**, 201500010.
11 (a) H. Yan, J. Yang, G. Ma, G. Wu, X. Zong, Z. Lei, J. Shi, C. Li. *J. Catal.,* 2009, **266**, 165. (b) J. S. Jang, S. H. Choi, H. G. Kim, J. S. Lee. *J. Phys. Chem. C,* 2008, **112**, 17200. (c) C. Han, M. Q. Yang, N. Zhang, Y. J. Xu. *J. Mater. Chem. A,* 2014, **2**, 19156. (d) Y. J. Zhang, L. Zhang. *Appl. Surf. Sci.,* 2009, **255**, 4863.
12 (a) J. Yang, D. Wang, H. Han, C. Li. *Acc. Chem. Res.,* 2013, **46**, 1900. (b) X. Fu, J. Long, X. Wang, D. Y. C. Leung, Z. Ding, L. Wu, Z. Zhang, Z. Li, X. Fu. *Int. J Hydrogen Energy,* 2008, **33**, 6484.
13 (a) J. Chen, X. J. Wu, L. Yin, B. Li, X. Hong, Z. Fan, B. Chen, C. Xue, H. Zhang. *Angew. Chem. Int. Ed.,* 2015, **54**, 1210. (b) L. J. Zhang, R. Zheng, S. Li, B. K. Liu, J. Wang de, L. L. Wang, T. F. Xie. *ACS appl. Mat. Interfaces,* 2014, **6**, 13406. (c) S. Cao, Y. Chen, C. J. Wang, X. J. Lv, W. F. Fu. *Chem. Commun.,* 2015, **51**, 8708. (d) Z. Sun, Q. Yue, J. Li, J. Xu, H. Zheng, P. Du. *J. Mater. Chem. A,* 2015, **3**, 10243. (e) J. Ran, J. Yu, M. Jaroniec. *Green Chem.,* 2011, **13**, 2708.
14 (a) Y. Li, Y. Hu, S. Peng, G. Lu, S. Li. *J. Phys. Chem. C,* 2009, **113**, 9352. (b) Y. Li, L. Tang, S. Peng, Z. Li, G. Lu. *Crystengcomm,* 2012, **14**, 6974.
15 (a) Y. Zhu, Z. Chen, T. Gao, Q. Huang, F. Niu, L. Qin, P. Tang, Y. Huang, Z. Sha, Y. Wang. *Appl. Catal. B Environ.,* 2015, **163**, 16. (b) G. Xin, B. Yu, Y. Xia, T. Hu, L. Liu, C. Li. *J. Phys. Chem. C,* 2014, **118**, 21928. (c) Y. Zhang, H. Liu, G. Zhang, L. He, P. Liu, B. Lin. *Mater. Res. Bull.,* 2014, **60**, 510. (d) G. Liu, C. Sun, H. G. Yang, S. C. Smith, L. Wang, G. Q. Lu, H.-M. Cheng. *Chem. Commun.,* 2010, **46**, 755.
16 (a) Y. Wang, Y. Wang, R. Xu. *J. Phys. Chem. C,* 2013, **117**, 783. (b) X. Wang, G. Liu, Z.-G. Chen, F. Li, L. Wang, G. Q. Lu, H.-M. Cheng. *Chem. Commun.,* 2009, 3452. (c) M. Luo, W. Yao, C. Huang, Q. Wu, Q. Xu. *J. Mater. Chem. A,* 2015, **3**, 13884. (d) X. J. Lv, W. F. Fu, H. X. Chang, H. Zhang, J. S. Cheng, G. J. Zhang, Y. Song, C. Y. Hu, J. H. Li. *J. Mater. Chem.,* 2012, **22**, 1539.
17 J. Jin, J. Yu, G. Liu, P. K. Wong. *J. Mater. Chem. A,* 2013, **1**, 10927.
18 M. Zhang, J. Xie, Q. Sun, Z. Yan, M. Chen, J. Jing. *Int. J Hydrogen Energy,* 2013, **38**, 16402.
19 (a) X. Wang, Z. Feng, D. Fan, F. Fan, C. Li. *Cryst. Growth Des.,* 2010, **10**, 5312. (b) J. Park, S. Park, R. Selvaraj, Y. Kim. *RSC Adv.,* 2015, **5**, 52737.
20 X. Jiang, X. Fu, L. Zhang, S. Meng, S. Chen. *J. Mater. Chem. A,* 2015, **3**, 2271.
21 J. Tauc, R. Grigorovici, A. Vancu. *physica status solidi (b),* 1966, **15**, 627.
22 C. Li, L. Han, R. Liu, H. Li, S. Zhang, G. Zhang. *J. Mater. Chem.,* 2012, **22**, 23815.
23 M. Berr, A. Vaneski, A. S. Susha, J. Rodríguez-Fernández, M. Döblinger, F. Jäckel, A. L. Rogach, J. Feldmann. *Appl. Phys. Lett.,* 2010, **97**, 093108.
24 (a) S. Xiong, E. B. Isaacs, Y. Li. *J. Phys. Chem. C,* 2015, **119**, 4834. (b) F. F. Schweinberger, M. J. Berr, M. Doblinger, C. Wolff, K. E. Sanwald, A. S. Crampton, C. J. Ridge, F. Jackel, J. Feldmann, M. Tschurl, U. Heiz. *J. Am. Chem. Soc.,* 2013, **135**, 13262.
25 (a) H. Zhao, Y. Dong, P. Jiang, G. Wang, H. Miao, R. Wu, L. Kong, J. Zhang, C. Zhang. *ACS Sustainable Chem. Eng.,* 2015, **3**, 969. (b) Y. Zhu, Y. Wang, Z. Chen, L. Qin, L. Yang, L. Zhu, P. Tang, T. Gao, Y. Huang, Z. Sha, G. Tang. *Appl. Catal. A Gen.,* 2015, **498**, 159.
26 V. Zunic, M. Vukomanovic, S. D. Skapin, D. Suvorov, J. Kovac. *Ultrason. Sonochem.,* 2014, **21**, 367.
27 Z. Rui, S. Wu, C. Peng, H. Ji. *Chem. Eng. J.,* 2014, **243**, 254.
28 T. Wang, H. Meng, X. Yu, Y. Liu, H. Chen, Y. Zhu, J. Tang, Y. Tong, Y. Zhang. *RSC Adv.,* 2015, **5**, 15469.
29 L. Shen, N. Bao, P. E. Prevelige, A. Gupta. *J. Phys. Chem. C,* 2010, **114**, 2551.
30 C. Roychowdhury, F. Matsumoto, V. B. Zeldovich, S. C. Warren, P. F. Mutolo, M. Ballesteros, U. Wiesner, H. D. Abruña, F. J. DiSalvo. *Chem. Mater.,* 2006, **18**, 3365.
31 E. Makotchenko, I. Baidina, S. Gromilov. *J Struct. Chem.,* 2007, **48**, 1156.
32 G. Dukovic, M. G. Merkle, J. H. Nelson, S. M. Hughes, A. P. Alivisatos. *Adv. Mater.,* 2008, **20**, 4306.

33 (a) L. Song, Y. Li, S. Zhang, S. Zhang. *J. Phys. Chem. C,* 2014, **118**, 29777. (b) J. Zhang, S. Z. Qiao, L. Qi, J. Yu. *Phys. Chem. Chem. Phys.,* 2013, **15**, 12088.
34 R. A. Damodar, S.-J. You, S.-H. Ou. *Sep. Purif. Technol.,* 2010, **76**, 64.

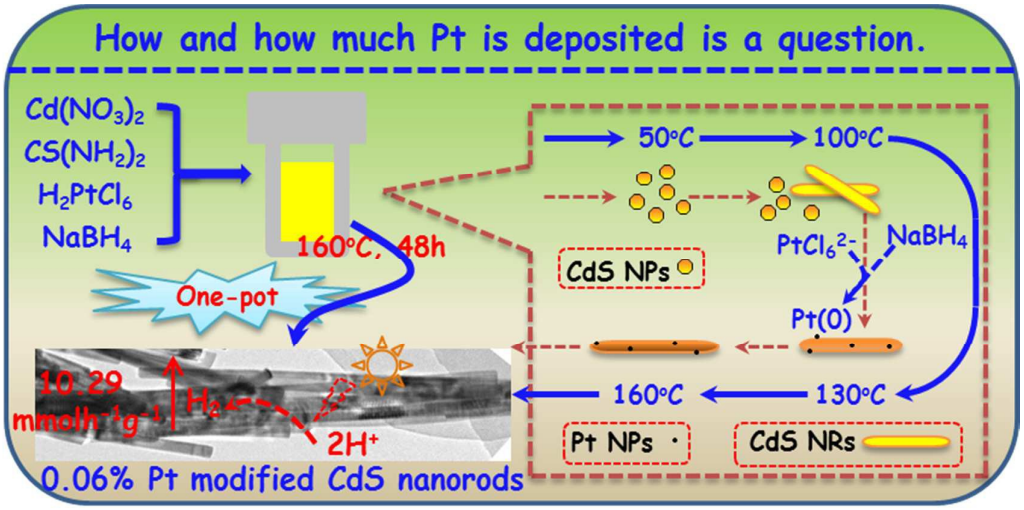

A simple and convenient one-pot solvothermal method was developed for the preparation of platinized CdS nanorods. The route is more efficient than the conventional post-deposition methods to enhance the photocatalytic HER activity of CdS. Furthermore, this work reveals that the using of noble metal co-catalyst can be significantly reduced (to only 0.06%) without unduly sacrificing the HRE activity.